Biofabrication

PAPER

Three-dimensional printing of a microneedle array on personalized curved surfaces for dual-pronged treatment of trigger finger

Seng Han Lim, Jian Yao Ng and Lifeng Kang

Department of Pharmacy, Faculty of Science, National University of Singapore, Block S4A, Level 3, 18 Science Drive 4, Singapore 117543

E-mail: lkang@nus.edu.sg

RECEIVED
2 September 2016

REVISED
1 November 2016

ACCEPTED FOR PUBLICATION
14 November 2016

PUBLISHED
10 January 2017

Keywords: 3D printing, microneedle array, transdermal drug delivery, personalized medicine, trigger finger

Abstract

The hand function of patients who suffer from trigger finger can be impaired by the use of traditional splints. There is also a risk of systemic side effects with oral non-steroidal anti-inflammatory drugs (NSAIDs) used for pain relief. Microneedle-assisted transdermal drug delivery offers an attractive alternative for local delivery of NSAIDs. However, traditional microneedle arrays fabricated on flat surfaces are unable to deliver drugs effectively across the undulating skin surface of affected finger(s). In this study, using 3D printing, a dual-function microneedle array has been fabricated on personalized curved surfaces (microneedle splint) for drug delivery and splinting of the affected finger. The novel microneedle splint was assessed for its physical characteristics and the microneedles were shown to withstand up to twice the average thumb force without fracturing. An average skin penetration efficiency of 64% on dermatomed human cadaver skin was achieved and the final microneedle splint showed biocompatibility with human dermal cell lines. A significantly higher amount of diclofenac permeated through the skin by 0.5 h with the use of the microneedle splint as compared to intact skin. The fabricated microneedle splint can thus be a potential new approach to treat trigger finger via personalized splinting without affecting normal hand function.

1. Introduction

Trigger finger is an inflammation of the finger joint which affects about 2% of the general population globally [1–3]. It is more common among women, especially in the fifth and sixth decades of life [4]. The mechanism of injury is postulated to be due to a disparity in the size of the flexor tendons and the enclosing sheath in the surrounding retinacular A1 pulley system which overlies the most commonly affected metacarpophalangeal (MCP) joint. The rest of the finger joints could also be affected [5–7]. This disparity in size could be due to fibrocartilaginous metaplasia of the flexor tendons as a result of repeated flexion and extension of the finger [6, 8–10]. The tendons become caught when they glide through the sheath [5, 11], resulting in locking of the affected finger(s) during flexion which requires painful manipulation into extension [12]. Some of the risk factors for trigger finger include repetitive finger movements, diseases such as diabetes and rheumatoid arthritis and local trauma [13]. The use of modern mobile devices, involving repetitive finger motion, has increased dramatically in recently years, with up to 97 per 100 people globally having a mobile cell phone subscription [14]. As such, the incidence of trigger finger may possibly increase in the near future.

The first-line therapy for primary trigger finger is oral non-steroidal anti-inflammatory drugs (NSAIDs) for pain relief [5, 13] and finger splinting for immobilization of the affected joint(s) [15–17]. The suggested duration of splinting is 3–6 weeks [15]. The traditional method of splinting involves taping a tongue blade over the affected finger and palm to hold the MCP joint of the affected finger at 10° to 15° of flexion with respect to the proximal interphalangeal (PIP) and distal interphalangeal (DIP) joints [18, 19].

However, the current first-line clinical therapy is plagued by the following challenges. Firstly, splinting requires a tongue blade to be taped onto the whole hand, which renders the hand functionally impaired for at least 3 weeks. Secondly, oral NSAIDs have a risk of systemic side effects that include drug interactions with anticoagulants, antiplatelets [20, 21],

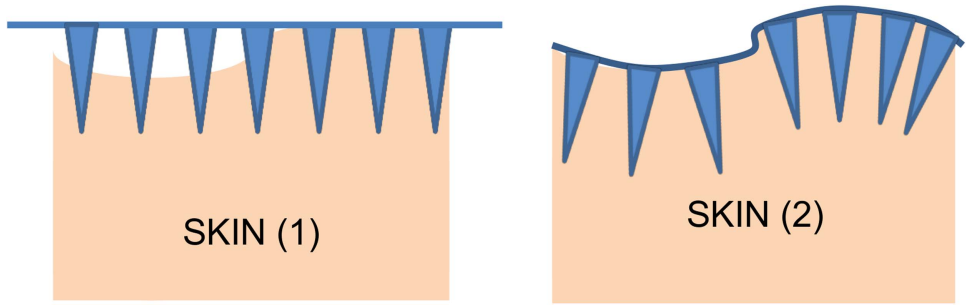

Figure 1. Schematic representation of a MN array on a flat surfaces and a MN array on a personalized contoured surface. SKIN (1) represents a MN array on a flat surface inserted on an undulating, uneven skin surface. SKIN (2) represents a MN array on a personalized curved surface, achieving complete insertion into the undulating human skin.

antihypertensives [22, 23], antidepressants [24–28], methotrexate [29] and others. Consumption of NSAIDs also increases the risk of cardiovascular, cerebrovascular [26, 30–33] and gastrointestinal adverse events, [34] and may precipitate renal [35–37] and hepatotoxicity [38–42]. Hence, the current treatment approach can potentially lower the quality of life of the patient.

Microneedle (MN)-assisted transdermal drug delivery offers an attractive alternative for NSAIDs to be delivered locally into the capillaries surrounding the affected joint(s), without significant systemic side effects [43, 44]. However, the surface of a finger is undulating and unique due to inter-individual differences in the structure of the finger joints, skin elasticity and the amount of hair on the skin. As such, Traditional MN arrays, which are fabricated on flat surfaces, are often not completely inserted and large amounts of loaded materials are not delivered [45]. Furthermore, traditional flat MN arrays are subjected to the 'bed of nails' effect where the force on each MN is equally distributed across the array. This results in the inability of all MNs to overcome the elasticity of the epidermis and puncture the skin. This can lead to suboptimal dosing and a huge wastage of drug incorporated into the MN array. One way to resolve this issue is to fabricate MN arrays that contour fully to human skin. This allows all the MNs to be inserted completely into the skin, as illustrated in figure 1. Current MN fabrication techniques adapted from the microelectronics industry [46] include a series of photolithography, thin-film deposition or dry and wet etching techniques [47], and are unable to effectively fabricate MN arrays on curved surfaces.

Several groups have attempted to fabricate MN arrays on a flat surface and superimpose them onto flexible patches [48–50] that curl around the skin upon application. However, the administration of these flexible patches is likely to be dependent on user expertise to ensure proper use. The flexibility of the patch may also be insufficient to account for minor indentations or variations of the skin. Finally, these fabrication techniques lack the ability to change design quickly and often involve multiple steps such as a tedious preparation of a master template followed by micro-molding.

Unlike traditional subtractive or formative manufacturing, additive manufacturing (AM) technology enables the construction of a sturdy physical model [51] of any geometrical complexity up to the micron scale, layer by layer until it is completely fabricated [52]. Furthermore, using computer-aided design (CAD) software for an AM technology such as three-dimensional printing (3DP), a personalized splint with a unique curved surface that contours the patient's finger can be designed. As such, 3DP could potentially fabricate MN arrays on the curved surface of a personalized splint as well as fabricate the splint itself in a single process.

In this study, we developed a MN array on personalized curved surfaces, or a MN splint via 3DP, that acts as a splint to immobilize the affected trigger finger and delivers NSAIDs through MN-assisted transdermal drug delivery [53, 54] for pain relief.

2. Materials and methods

2.1. Materials

Trypan blue, diclofenac sodium and phosphate-buffered saline (PBS) powder were purchased from Sigma-Aldrich (St Louis, MO, USA). PrestoBlue® was obtained from Invitrogen (Carlsbad, CA, USA). Culture media consisted of Dulbecco's Modified Eagle Medium (DMEM) (Invitrogen) supplemented with 10% of fetal bovine serum (FBS) (Invitrogen) and 1% of 10 000 U ml^{-1} penicillin and 10 mg ml^{-1} streptomycin (PS) (PAN-Biotech GmbH, Germany). 3DM-Castable resin was purchased from Kudo3D Inc. (Pleasanton, CA, USA). 10% neutral buffered formalin was purchased from Leica Biosystems Nussloch GmbH (Germany). All other reagents were of analytical grade.

2.2. Design of the MN splint

A human hand CAD model was obtained from an online source to simulate that of an actual patient. The

CAD software used for the entirety of this study was AutoCAD© 2016 (Autodesk® Inc., San Rafael, CA, USA). A splint model was designed to fit snugly to the finger, based on the contours and dimensions of the hand model, via AutoCAD© 2016. Subsequently, arrays of MNs were created on the splint's inner contoured surface. The MNs were designed to have 300 μm base diameter and a 1800 μm center-to-center spacing [55]. The MN height was set at 900 μm to achieve penetration through the skin on the palm [56]. Two rings were attached to the splint to allow the user to wear the splint instead of needing to tape the splint to the finger.

2.3. Fabrication of the MN splint

A commercial Digital Light Processing or DLP 3D printer (Titan1, Kudo3D Inc.) equipped with a Viewsonic® DLP projector was utilized for printing the MN splint. The individual images used for fabrication were processed by Creation Workshop Envision Labs (St Mankato, MN, USA) into 50 μm layers, exported and opened as a zip file in Titan1's control software. The printer *XY* resolution was set as 50 μm. Two MN splints were printed at the same time to reduce the total operation time. A proprietary resin, 3DM-Castable, was used for the fabrication. Light spectra of the DLP projector used was measured using an optics spectrometer (USB4000-XR1, Ocean Optics Inc., FL, USA).

2.4. Post-fabrication treatment

The printed MN splint was peeled off slowly from the build platform and subjected to a series of rinsing. Firstly, the printed splint was soaked in an organic solvent (isopropyl alcohol), with a change of fresh solvent every 15 min until there was no coloration to the solvent. Excess solvent was rinsed off with tap water and left to dry. Subsequently, the fabricated MN splint was exposed to UV–vis light at 400 nm under a post-curing LED lamp to cure any remaining uncured resin for a total of 2 h. The MN splint was then soaked in PBS for 24 h, with a change in PBS after 12 h, and finally soaked in 70% v/v ethanol for 24 h, with a change in ethanol after 12 h. The MN splint was left to dry before use.

2.5. Test of fracture force

MNs experience both axial and shear fracture forces [57]. Therefore, the MN arrays were subjected to compression forces in all three directions in the *X*-, *Y*- and *Z*-axes before the percentage breakage of MNs can be concluded. The MNs at the top, center and bottom of a MN splint (see figure 4(D)) were first observed, demarcated and photographed using a Nikon SMZ25 stereomicroscope (Nikon, Japan) and the measurement tools of Nikon imaging software (NIS-Element Analysis D 4.20.00) to obtain 'before' images. Subsequently, a Algol JSV H1000 digital force gauge (Algol Instrument Co. Ltd., Taiwan) was used to compress the MN splint against a printed finger model, made of acrylonitrile butadiene styrene (ABS), for 30 s at a thumb force of ~20 N [58] in the *Z*-axis as designated in figure 4(Eiii). MNs at the same locations were photographed using the same stereomicroscope to obtain 'after' images. The 'before' and 'after' images of the MNs were compared for visual inspection of any fracture. The percentage of intact MNs after compression was then determined. The test was conducted in triplicate. Subsequently, the whole experiment was repeated at compression forces of 30 N and 40 N. After completing the test of fracture force for the *Z*-axis, the entire experiment was repeated for both the *X*- (figure 4(Ei)) and *Y*-axes (figure 4(Eii)).

2.6. Skin preparation

Human dermatomed skin was obtained from Science Care (Arizona, USA). The skin tissues were excised from the thighs of a Caucasian female donor aged 92. Visual inspection was performed prior to the experiment to ensure there was no breakage in the skin tissue and its skin barrier function.

2.7. Skin and MN penetration

A polydimethylsiloxane (PDMS) replica of the finger model was previously prepared to mimic full-thickness skin. Briefly, a mixture of silicone elastomer base and silicone elastomer curing agent at a weight ratio of 9:1 was poured into a 3D-printed reverse mold of the finger model. The mixture was degassed before being heat cured at 70 °C for 2 h. Dermatomed human cadaver skin was placed over the PDMS finger substrate and a MN splint was placed onto the skin to complete the setup. The setup was then taped with Leukoplast®. Subsequently, the MN splint was compressed onto the skin using a thumb with slow rotational motion for 3 min across the MN splint to achieve penetration of the MNs.

2.8. Skin penetration efficiency test

The percentage of successful MN penetration was determined by a trypan blue staining method. After application of the MN splint, the skin was flooded with trypan blue solution for 10 min. The skin was later cleansed with distilled water, followed by 70% v/v ethanol. The stained human cadaver skin was photographed using a Nikon SMZ25 stereomicroscope and the penetration efficiency was analyzed.

2.9. Histological examination

The MN-treated skin samples were fixed with 10% neutral buffered formalin for 48 h and subsequently transferred to 15% sucrose solution 24 h before sectioning. Immediately before sectioning, the skin samples were frozen in the embedding matrix with liquid nitrogen and separately cross-sectioned using the cryostat (CM3050 S, Leica, Germany) to obtain

cross-sections of 10 μm. The cross-sections were stained as per standard protocols of hematoxylin and eosin (H&E) staining. The obtained stained samples were imaged and analyzed using the Nikon SMZ25 stereomicroscope.

2.10. *In vitro* biocompatibility of DLP-printed parts

The test for biocompatibility was designed based on EN ISO 10993-12:2012 guidelines. Three 1 cm^3 cubes were previously printed and subjected to the post-fabrication treatment. A total of 6 ml of PBS was subsequently used to soak the cubes for 24 h to extract any substances which may leak from the printed parts.

Human dermal fibroblast (HDF) and human adult low calcium high temperature (HaCaT) cells were used to assess the toxicity of the polymer used in 3D printing. Cells were grown in DMEM supplemented by 10% FBS and 1% penicillin–streptomycin solution. Ten thousand cells were plated into 96-well microtiter plates in 200 μl of culture medium. After 24 h of incubation at 37 °C and 5% CO_2, all culture medium was removed and replaced with 180 μl of fresh culture medium and 20 μl of extract for each well. The negative control consisted of wells containing 180 μl of fresh culture medium and 20 μl of sterile PBS. The plates were incubated at 37 °C and 5% CO_2 for 24 h and 72 h.

At the respective time points, 22 μl of PrestoBlue® cell viability reagent was pipetted into each of the wells. The 96-well plate was then incubated for 30 min under the same incubation conditions stated above. Finally, the absorbance of the wells was analyzed with an absorbance plate reader (SpectraMax® 190, Sunnyvale, CA, USA) at a wavelength of 570 nm with a reference wavelength of 600 nm. This utilizes the reducing power of metabolically active cells to reduce resazurin to resorfin, with wavelengths of maximum absorbance of 600 nm and 570 nm, respectively. A higher absorbance readout of 570 nm over 600 nm indicates the presence of viable cells. The 570 nm absorbance readings will be subtracted from the 600 nm readings for all treated wells to obtain the normalized absorbance.

The normalized background absorbance of resorfin was determined from the blanks and subtracted from the normalized absorbance of the experimental and standard reference wells to obtain the corrected absorbance. Subsequently, the corrected absorbance of the experimental wells was expressed as a percentage of that of the control to determine the relative cell viability.

2.11. *In vitro* skin permeation of diclofenac gel using 'poke and patch'

Vertical Franz diffusion cells with an effective exposed area of 1 cm^2 were used. Skin samples pre-treated with the MN splint were mounted onto Franz diffusion cells with the epidermis facing up. Intact skin was used as a control. The donor cell contained about 2 g of commercially available diclofenac diethylamine 1.16% gel (Voren®, YSP Industries, Selangor, Malaysia) while the receptor cell contained 4.8 ml of 1× PBS. The cells were placed inside a hot air chamber with the temperature controlled at 32 °C. Magnetic stirrers in the receptor cells stirred at a speed of 180 rpm. The receptor solution was subjected to HPLC measurement of diclofenac diethylamine permeated through the skin at time points of 0.5, 1.5, 3, 6, 9.75, 21 and 24 h.

2.12. Drug analysis

The amount of diclofenac diethylamine permeated was determined by using Hitachi L2000 LaChrome Elite HPLC system with an Agilent Eclipse XDB C18 column (4.6 mm × 150 mm × 5 μm, 80 Å). The mobile phase consisted of mobile phase A (10 mM potassium dihydrogen phosphate, adjusted to pH 6.3) and mobile phase B (100% acetonitrile) with an isocratic elution program with ratios of solvents A:B of 60:40. The flow rate was set at 1 ml min^{-1}. The injection volume was 20 μl for each sampling and ultraviolet detection was performed at a wavelength of 282 nm. A calibration curve was constructed using the respective standard solutions from 60 ppb to 250 ppm.

2.13. Data analysis

All results were collated, analyzed and presented as mean ± standard deviation. All statistical analysis was performed by descriptive statistics or independent sample *t*-tests using IBM SPSS Statistics 21.0 (IBM, New York, USA). A probability value of $p < 0.05$ was considered statistically significant. All graphical outputs were analyzed and produced by OriginPro 2015 (Northhampton, MA, USA).

3. Results

3.1. Design and fabrication of the personalized dual-function MN splint

Design of the personalized dual-function MN splint was achieved using CAD software (details are given in section 2). Briefly, a CAD hand model to simulate the clinical patient was superimposed onto a pre-designed splint (figure 2(Ai)). The overlapping region was virtually subtracted to produce a personalized contoured surface on the inner surface of the splint (figure 2(Aii)). MNs were implanted onto the personalized contoured surface (figure 2(Aiii)) and the connecting rings were sliced open to allow easier wearing by the patient. The base of splint was also trimmed to reduce unnecessary weight (figure 2(Aiv)). The completed CAD model was then digitally sliced into layers of thickness 50 μm and sent for printing. Fabrication of the MN splint was achieved via a Digital Light Processing 3D printer (DLP) with a proprietary resin (figure 2(B)). Briefly, light rays ranging from 400 nm

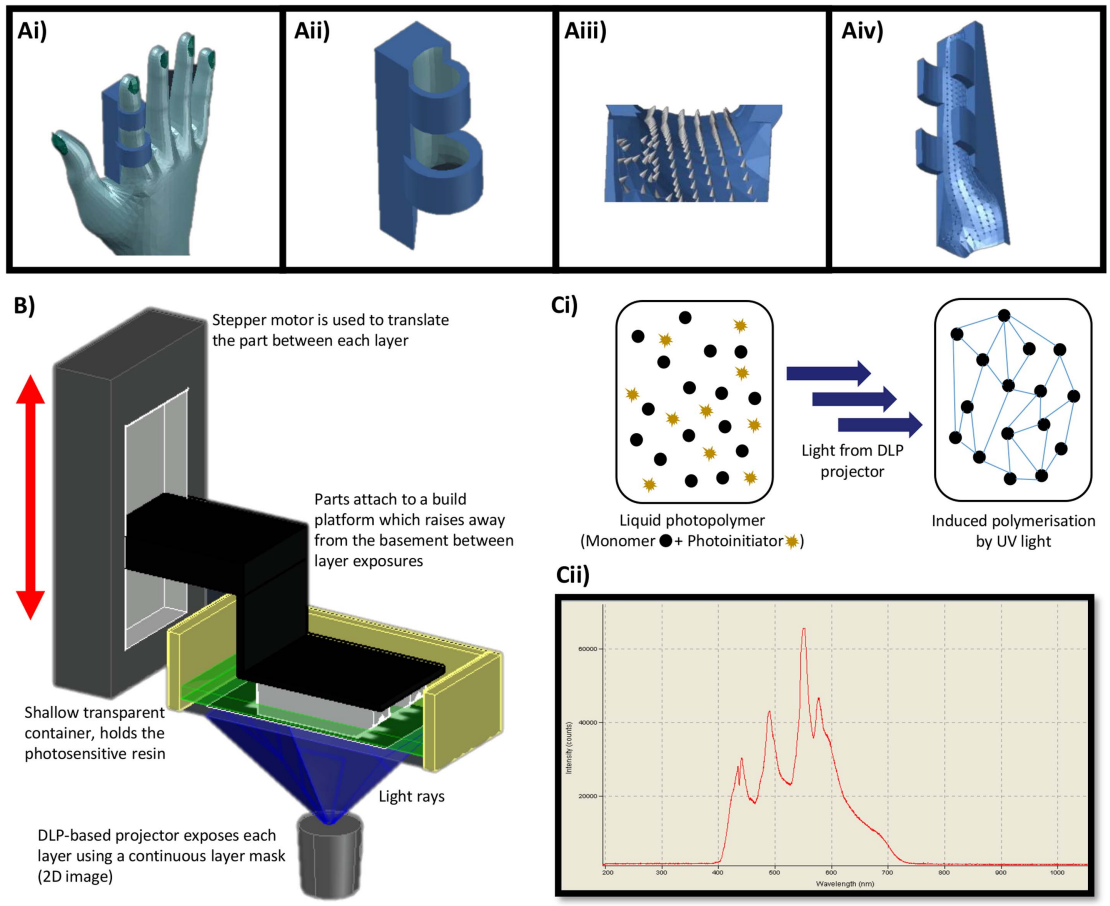

Figure 2. Design and fabrication process of the personalized microneedle (MN) splint. (A) The various design steps. (Ai) 3D model of a human adult hand superimposed with a typical splint. (Aii) 3D model of a MN splint with an internal surface that is fully contoured to the human hand. (Aiii) Virtual grafting of MNs onto the personalized contoured surface of the MN splint. (Aiv) 3D model of a final MN splint, ready for fabrication. (B) 3D printing of the MN splint using stereolithography, enhanced with digital light processing technology to turn liquid resin into a solid MN splint. Careful selection of resin is done to ensure biocompatibility of the printed MN splint to human skin. (Ci) Schematic diagram to illustrate photopolymerization of the resin from liquid into a solid of the desired pattern. (Cii) Light spectrum of the DLP projector light source.

to 700 nm (figure 2(Cii)) from the DLP projector were projected in a 2D image according to the design. Photopolymerization occured in which monomers undergo free radical polymerization to form a mesh network joining them together, transforming from liquid to solid state in the desired pattern as per the sliced images (figure 2(Ci)). This process was repeated as soon as the build platform returned to its previous height and continues until the entire model was built. Once completed, a series of post-processing treatments are done to remove any residual resin. Details of the post-processing treatment are given in section 2.

3.2. Fabricated MN splint

The basic printing parameters of Titan1 were optimized to enable the printing of two splints in 1 h 45 min. Analysis of the fabricated MN splint showed that there were 238 MNs fabricated, as designed. The 3D-printed MN splint had a measured length of 7 cm (figures 3(A), (B)) and a width of 2 cm (figure 3(C)). The resulting MNs have a base diameter of ~600 μm, tip diameter of ~50 μm and height of ~800 μm (figure 3(F)). The center-to-center spacing was ~1800 μm (figure 3(E)). When fitted onto the index finger of the 3D-printed hand model, the rings provided grip and prevented slipping of the MN splint. The inner surface of the MN splint was fully contoured to the curvature of the finger as designed. The end ring gaps allowed the MN splint to be fitted onto the index finger without the need to slide the finger across the MNs (figure 3(D)).

3.3. Fracture force test

At various locations on the splint (top, center and bottom) 87–99% of MNs remained intact after different forces of compression were applied at the three main axes, *X*, *Y* and *Z* (figure 4). Consistently, the highest number of MNs which remained intact after compression at all forces, for all three directions, were located at the center of the MN splint. There was no significant difference between the percentage of MNs which remained intact after the compression forces at each of the three different directions. This could be

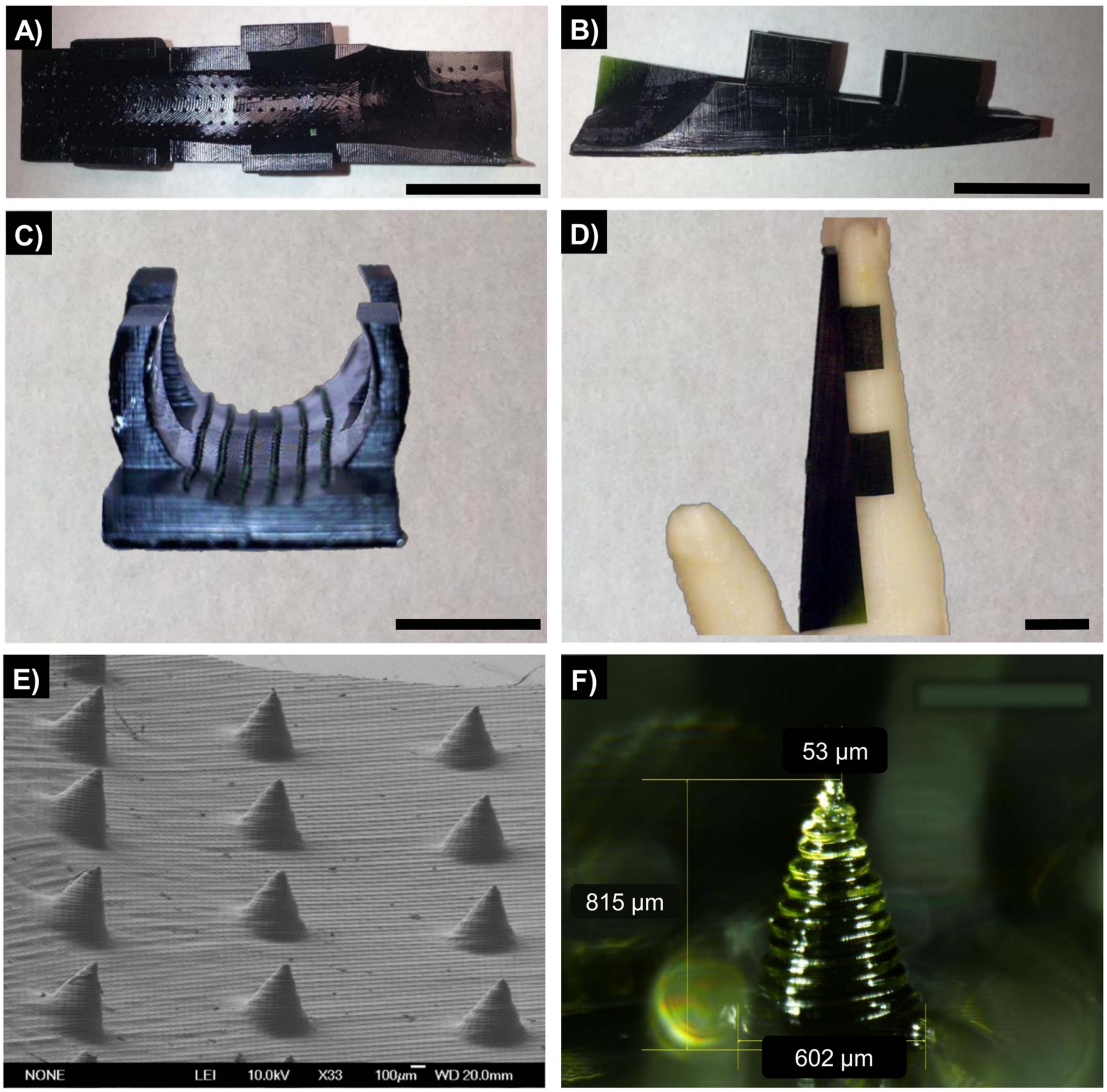

Figure 3. Images of the microneedle (MN) splint. (A) Top view of the MN splint (scale bar = 2 cm). (B) Side view of the MN splint (scale bar = 2 cm). (C) Top view of the arrays of MNs 3D-printed on the inner surface of the MN splint (scale bar = 1 cm). (D) Side view of the MN splint fitted onto the hand model (scale bar = 1 cm). (E) SEM image of MNs on a personalized contoured surface of the MN splint (F) A single MN on personalized contoured surface.

due to the increase in shear resistance of MNs attributed to their geometry with a ~1.3 aspect ratio of height to base diameter [59]. Results of the fracture force test indicated that MNs fabricated via this 3DP method would not fracture under the typical thumb force, which was the amount of force subsequently used to effect penetration through the skin.

3.4. Skin penetration efficiency

Figure 5 illustrates the successful penetration of MNs through human cadaver skin along different sections of the MN splint (top, center and bottom). Micropores created in the cadaver skin were stained with trypan blue (figures 5(B)–(D)), a dye specific to the sites of perforation of the stratum corneum. The number of stained holes was counted and an average skin penetration rate of 63.7% (±30.5%) was achieved, out of three replicates. Histological sections with H&E staining are shown in figures 5(E)–(F), specifically with the MN-punctured pores highlighted in red. Within the punctured pores, a breakage in the continuous stratum corneum and viable epidermal layer was observed which indicated successful penetration of the MNs through the outermost layer of the skin. Figure 5(A) and the highlighted box of figure 5(E) illustrate the microscope image and histological sections of an intact skin, respectively.

3.5. *In vitro* drug release of a NSAID using 'poke and patch'

Enhanced delivery of diclofenac diethylamine, using a commercial topical 1.16% gel, was observed after pretreatment of the skin sample with the fabricated MN splint (figure 6), compared with intact skin. This enhancement was greater at the initial stage of drug release. At 0.5 h, a significantly higher amount of cumulative diclofenac diethylamine in the receptor solution (p-value = 0.03) was observed for the MN

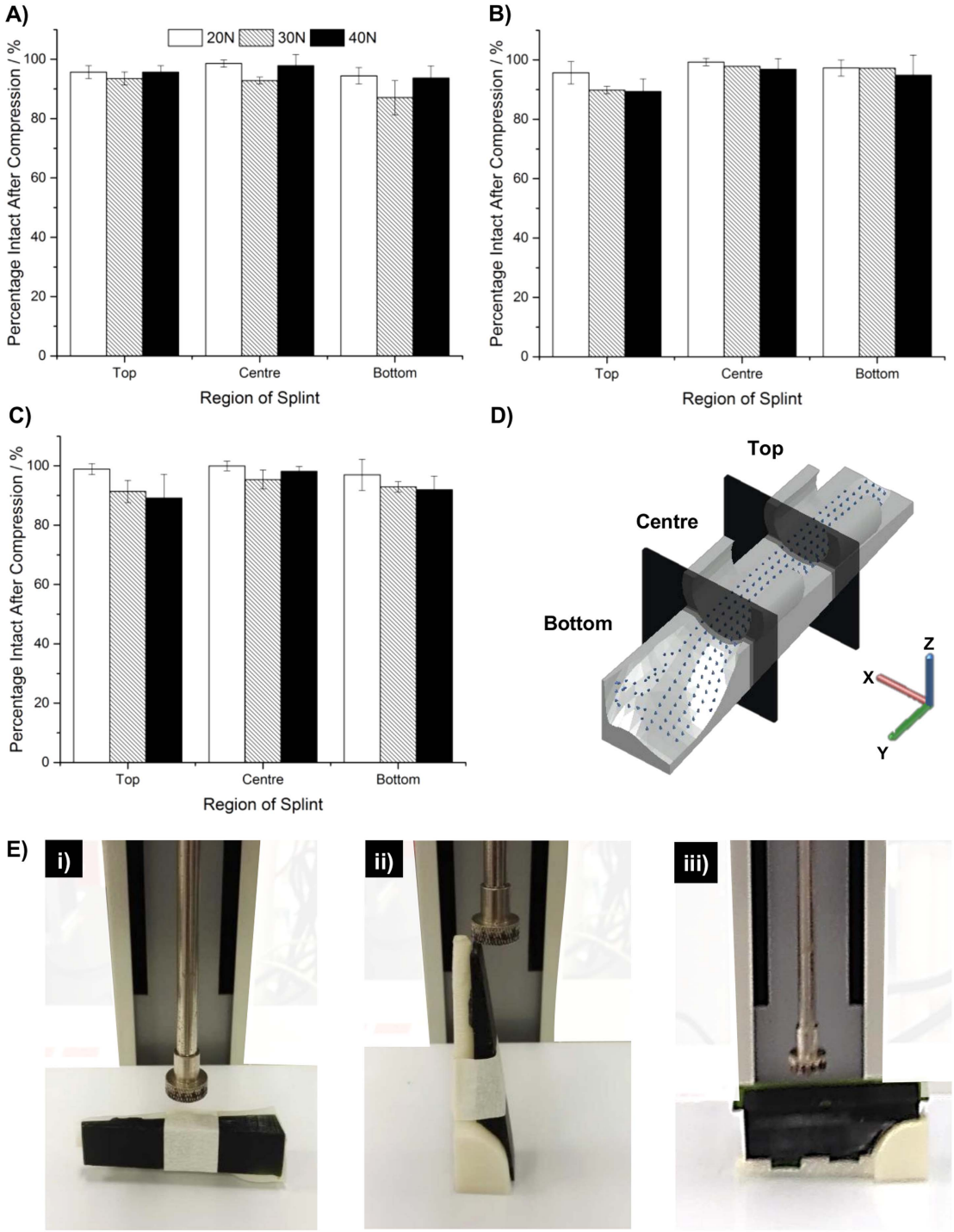

Figure 4. Mechanical strength testing for the microneedle (MN) splint. (A)–(C) Bar graphs for percentage of MNs which remained intact after different compression forces (20, 30 and 40 N) were applied from three different directions (*X*-, *Y*- and *Z*-axes), respectively. (D) Schematic showing the different regions of the MN splint (top, center and bottom) with respect to the three different directions (*X*-, *Y*- and Z-axes). (E) The MN testing setup using an automated force gauge, with the splint placed on a finger model 3D-printed using acrylonitrile butadiene styrene. (Ei) Fracture test from the *X*-axis; (Eii) fracture test from the *Y*-axis; (Eiii) fracture test from the *Z*-axis. In general, the MNs have good mechanical strength and over 90% of the MNs remained intact at twice the average thumb force of 40 N.

splint arm (~1.2 μg cm^{-2}) compared with the intact skin arm (~0.03 μg cm^{-2}). At 1.5 h, a significantly higher amount of cumulative diclofenac diethylamine in the receptor solution (p-value < 0.01) was observed for the MN splint arm (~4.0 μg cm^{-2}) compared with the intact skin arm (~0.9 μg cm^{-2}). This difference was approximately five times greater than the amount of diclofenac diethylamine that permeated through the intact skin arm. For the rest of the duration of the experiment, a consistently higher amount of cumulative diclofenac diethylamine in the receptor solution was observed for the MN splint arm compared with the intact skin arm; however, this difference was not statistically significant.

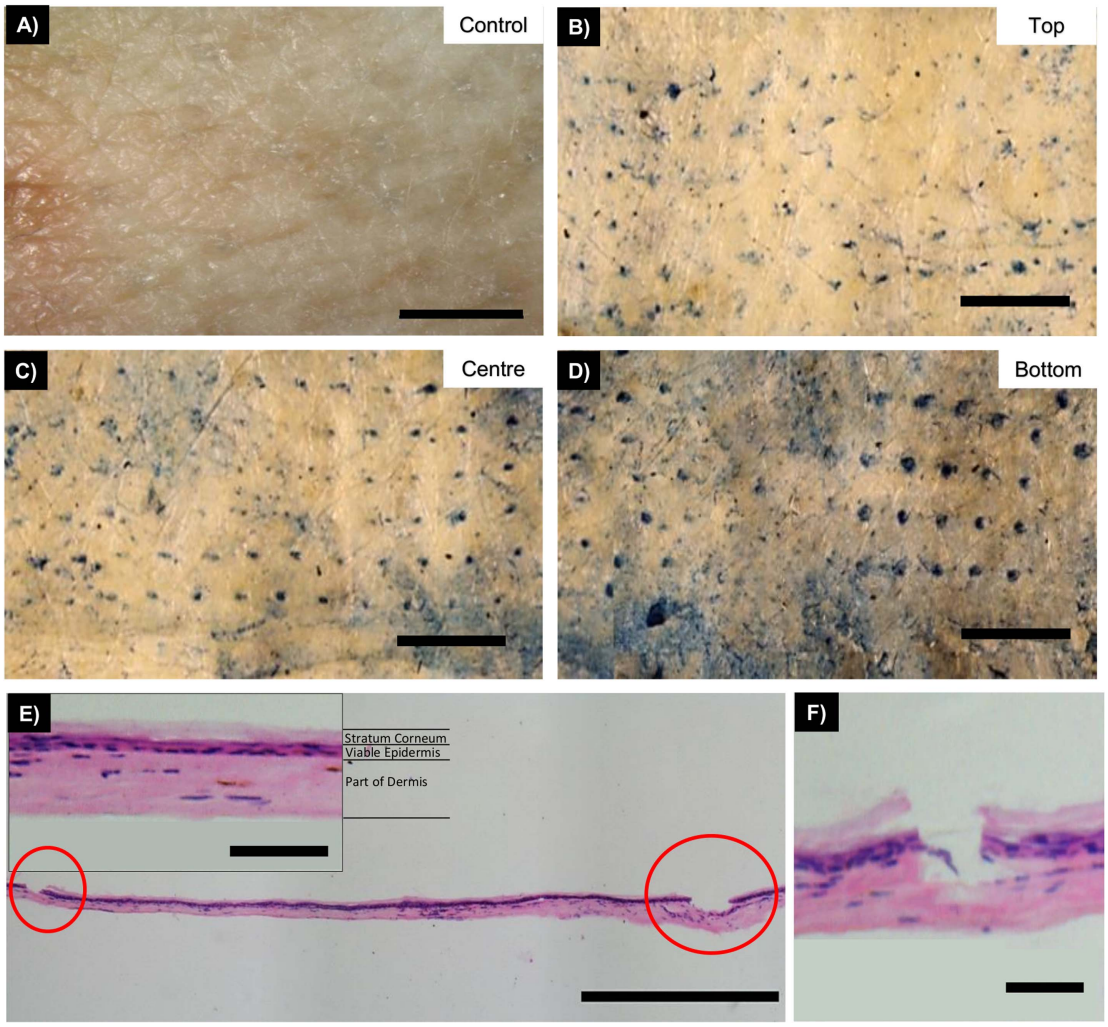

Figure 5. Microscope images of human cadaver skin used for the skin penetration efficiency test. (A) Skin sample before microneedle (MN) splint treatment (scale bar = 100 μm). (B) Skin sample after MN splint (top) treatment, with trypan blue staining (scale bar = 5 mm). (C) Skin sample after MN splint (center) treatment, with trypan blue staining (scale bar = 5 mm). (D) Skin sample after MN splint (bottom) treatment, with trypan blue staining (scale bar = 5 mm). (E) Histology image of H&E stained skin sample (with two MN-created pores in a row, circled in red) (scale bar = 500 μm) and a zoomed in image of intact skin (scale bar = 50 μm). (F) Histology image of H&E stained skin sample (scale bar = 50 μm).

3.6. Biocompatibility test

PrestoBlue® reagent, a resazurin-based solution, was used as an indicator of cell viability to compare the relative cell viability of dermal cell lines treated with extracts of the MN splint and those without, up to an incubation period of 72 h.

A relative cell viability of more than 100% (figure 7) was observed for both HDF and HaCaT keratinocytes up to 72 h of incubation with the extracts of the MN splint, as compared with those without. This indicated that the printed MN splint, subjected to post-fabrication treatment, was non-cytotoxic to the human dermal cells and was biocompatible.

4. Discussion

The novelty in our research lies in our group being the first to fabricate MNs directly onto curved surfaces rather than simple flat surfaces. Several groups have acknowledged that human skin is undulating and a simple flat planar MN array can possibly lead to problems such as incomplete insertion of MNs or suboptimal dosing when used on human skin [45]. In addition, this is the first time that the fabrication of MNs has been personalized to a specific patient (or, in this case, a specific model). This method can be used simultaneously with medical imaging techniques to fabricate a patient-specific MN array for both comfort and efficacy. Through the use of CAD software, patient-specific surfaces were created by subtracting the patient model from a pre-designed block, instead of using pre-determined sizes (e.g. small, medium or large) to fit different patients. This approach, while not uncommon in architecture, is relatively new in the field of medicine and paves the path for personalized medicine. Finally, unlike the fabrication of MNs on a flat surface using a 3D printer, as performed by Lu *et al* [60], fabrication of MNs on curved surfaces is faced with challenges such as overhanging MNs or MNs that

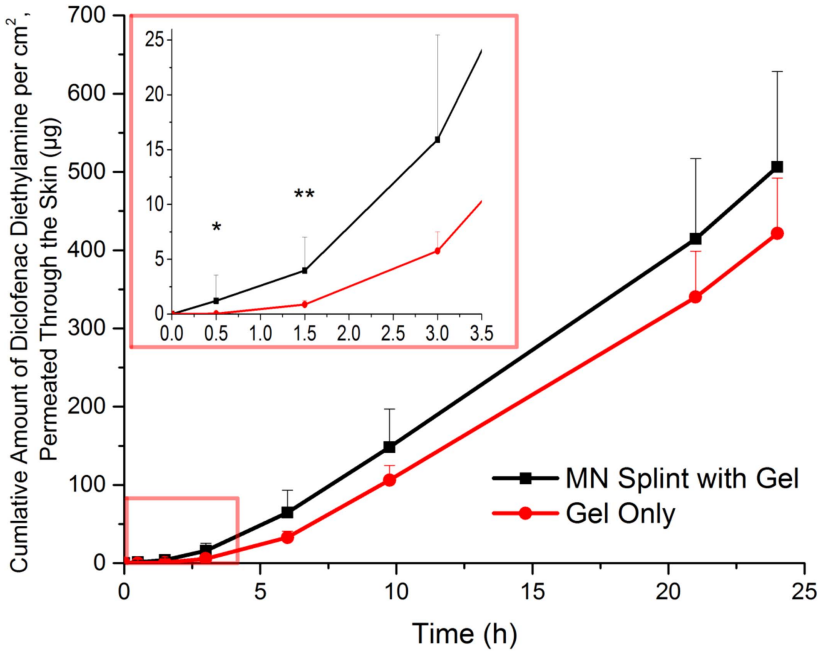

Figure 6. Cumulative release curve of diclofenac diethylamine across the skin for 24 h. Red box: zoomed in view of the cumulative release curve over the first 3 h. *Significant difference of $p < 0.05$. **Significant difference of $p < 0.01$.

bend out of plane. In our current research, we have demonstrated the use of a relatively inexpensive Digital Light Processing 3D printer to fabricate MNs not just on flat simple surfaces but also on curved surfaces, overcoming the challenges mentioned above.

In this study, a dual-function MN splint was fabricated. MNs were fabricated on a personalized contoured surface that fully adhered to the affected finger instead of on a flat planar surface. Other than immobilizing the affected finger, MNs fabricated on the splint were also demonstrated to have sufficient mechanical strength to prevent fracturing within the skin layers upon insertion of the MNs (up to twice an average thumb force) and achieved a skin penetration efficiency of 64%. When used together with a commercial topical gel, the MN splint demonstrated an enhanced delivery of diclofenac, up to five times the amount permeated through the skin by 1.5 h compared with intact skin alone. The 3D-printed MN splint demonstrated non-cytotoxicity to human dermal cell lines after a series of post-fabrication treatments.

It has been reported that a response to treatment for pain was detected in more than half of patients within 1 h of application of a commercial topical diclofenac diethylamine 1.16% gel [61]. Therefore, the amount of diclofenac permeated into the skin in 1 h from the commercial topical gel was considered as an approximate to the therapeutic level of diclofenac (estimated to be about 0.5 μg cm^{-2}). A similar method for determining the therapeutic level has been used by Zhang *et al* [62] in the case of lidocaine. The *in vitro* skin permeation test demonstrated that the MN splint pre-treatment group achieved a level of 1.2 μg cm^{-2} at 30 min (figure 6). Based on simple linear extrapolation, the therapeutic level of 0.5 μg cm^{-2} could be achieved at approximately 12 min for the MN splint pre-treatment group. This is evidence of the fast onset of therapeutic pain relief with the use of a MN splint together with a commercial topical diclofenac gel.

A skin penetration efficiency of 64% was achieved using the fabricated MN splint on dermatomed human cadaver skin. This appeared to be less than the average skin penetration efficiencies of >90% in other MN arrays [45] and therefore did not fit the hypothesis of having improved, if not complete, skin penetration for MNs fabricated on a personalized curved surface. However, this could have been due to the unknown thickness of the skin samples that were used in the assessment. During the design phase of the MN splint, the inner surface of the splint was designed to fully contour to the hand model. However, for the skin penetration study, an additional human skin sample was placed over the hand model. The unknown thickness of this skin has disrupted the contouring of the MN splint onto the hand model. In the actual application of an MN splint in clinical patients, a full scan of the affected hand together with the thickness of the skin will be done to create the basic CAD model. The subsequent full contouring of the MN splint onto the affected finger can then be fabricated. Furthermore, the high skin penetration efficiencies of other MN arrays were achieved with hairless pig cadaver skin. Human cadaver skin, which is generally more resistant to penetration by MNs, was shown to only achieved around 70% skin penetration [63].

In terms of safety, biocompatibility results demonstrated that the MN splint was safe for use after a series

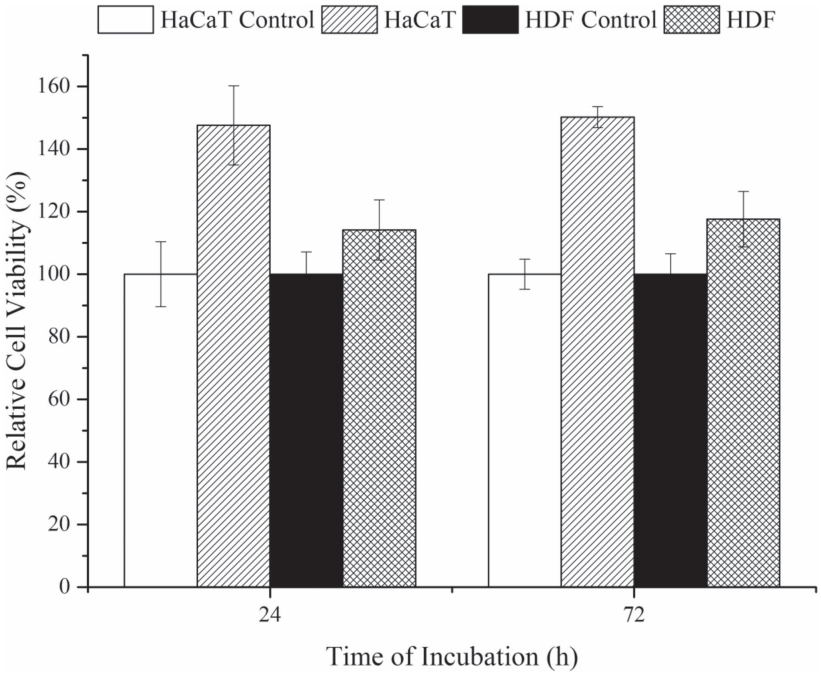

Figure 7. Relative cell viability of HaCaT keratinocytes and HDF cells as a percentage of their controls after 24 h and 72 h of incubation with Titan1 STL-printed polymer extract. Values are shown as means ± standard deviation. Both cell lines at 24 h and 72 h showed a relative cell viability of more than 100%.

of post-fabrication treatments. Of the MNs that broke during mechanical strength testing, only the very tip of the needles was broken. The broken tip stayed on top of the needle instead of being displaced from the needle. Therefore, it is hypothesized that should the needles break after insertion, most, if not all, of the broken tips will stick with the needles and be removed when the MN splint is removed from the finger. In the rare event that the broken tip stays in the skin, the non-toxicity of the MNs, as demonstrated by the biocompatibility data, will allow the tip to stay in the skin without causing irritation. The skin will expel the small broken tip over time. Furthermore, the MN splint has good mechanical strength, as demonstrated in figure 4, and the ~1.3 aspect ratio of MN height to base diameter could have contributed to its high mechanical strength [59], resulting in a lower risk of breakage of MNs in the skin.

The MNs were designed to have a 300 μm base diameter, 1800 μm center-to-center spacing and a height of 900 μm to achieve penetration through the skin on the palm. However, the final dimensions of the MNs, as illustrated in figure 3, were a tip diameter of ~50 μm, base diameter of ~600 μm, a height of ~800 μm and a center-to-center spacing of 1800 μm. The most obvious difference in the dimensions was that of the base diameter. This larger than designed diameter was probably due to an increase in exposure time of the resin in order to fabricate a layer that was strong enough to resist any breakage when the build platform was lifted from the resin container. This increase in exposure time may have caused a bigger area to be polymerized as the generated free radicals spread apart. The 3D printer used was a bottom-up DLP printer. This meant that the closer the layer was to the build platform, the greater the vacuum force experienced by the layer during separation of the build platform from the resin container. Since the base of MNs was nearer to the build platform during fabrication, an increase in exposure time of the resin to increase the strength of the printing layer was required to prevent the printing layer from breaking during separation of the build platform and the resin container. We acknowledge this to be a limitation of the current 3D printer used.

As the final printed MNs uniformly and repeatedly had a base diameter of ~600 μm, it was therefore possible to fabricate a MN with smaller base diameter if necessary by using a design with smaller base diameter. However, this adjustment was not made as the resultant MN geometry had an aspect ratio of approximately 1.3 (height to base diameter) and could be critical in providing resistance to shear fracture. There were also minimal dimensional changes to the MNs after the cleaning processes. Since the MN dimensions after post-fabrication treatment were uniform throughout the MN splint, the resulting MN splint was used for subsequent testing.

Liquid-based 3DP techniques such as DLP have been used increasingly in tissue engineering [64, 65] and other medical applications [66]. In terms of drug delivery, other than tablets for oral administration of drugs, MNs have also been fabricated previously by Lu *et al* [60] using similar technology with poly

(propylene) fumarate. However, their attempt was for MNs on flat planar surface. From our study, DLP was demonstrated to be a suitable technique for the fabrication of the MNs on personalized contoured surfaces, due to its high precision and fine resolution up to micron size. Software such as Materialise Mimics® can convert magnetic resonance imaging or computed tomography scans of clinical patients into working CAD models for the development of personalized medical devices. Together with the recent development of increasingly high-resolution 3D printers with greater speed and better precision, yet lower cost [67], it is likely that the fabrication of MNs on personalized contoured surfaces will increase for the treatment of clinical conditions in the next few years.

Our pioneering study in this field has culminated in a novel treatment approach for trigger finger that could potentially eliminate the need for patients to consume oral NSAIDs and endure traditional splinting. As this approach allows for localized delivery of drug [44], physicians could attempt to initiate NSAID therapy on patients with contraindications to systemic NSAIDs instead of having to use second-line corticosteroid injections. The MN splint only needs to be patched once a day and due to its safety profile, it could be self-administrated by patients. This could improve the compliance of patients with therapy. When a patient is diagnosed with trigger finger his or her hand model would be obtained with a 3D scanner. Next, individualized MN splints would be fabricated based on the patient's hand model and packaged into blister packs. Using a novel 'poke and patch' approach, the affected finger would first be 'patched' with a NSAID liquid formulation and a MN splint would be applied on the finger to perforate the stratum corneum, or 'poked', for transdermal delivery of the NSAID. Sufficient splints would be supplied to last the patient for at least 3 weeks with a daily change of the MN splint. Additional splints could be purchased as an over-the-counter (OTC) supply from the pharmacy that supplied the original quantity of splints.

Furthermore, the current MN splint has no drug embedded within it and could therefore be more quickly approved by the regulatory authorities for commercialization (compared with new drugs) which will improve the current clinical practice and benefit patients. The same method of fabrication has the potential to embed drugs into a MN splint for sustained and controlled release of drugs either via surface coating of MNs or by the addition of drug into the pre-polymerized resin before the MN splint is fabricated.

Other than the treatment of trigger finger, the fabrication of MNs on personalized contoured surfaces could be a platform technology for the treatment of other diseases that occur on or near the skin surface and are centered on a particular body part. The most prominent examples include rheumatoid/osteoarthritis or gout that occur in the joints. Other examples include alopecia or facial wrinkles, occurring on the scalp and face, respectively. 3DP fabricated MNs on personalized contoured surfaces could also provide opportunities for development of wearable bio-sensing devices. Wearable technologies such as watches could potentially incorporate hollow MN on the personalized contoured surfaces for bio-sensing (i.e. minimally invasive detection of electrolytes or other biomarkers in the body).

5. Conclusion

We have developed a personalized, dual-function MN splint via 3DP that can act as a splint to immobilize the affected trigger finger and deliver NSAIDs through MN-assisted transdermal drug delivery. In the future, diclofenac could be delivered through MN-assisted transdermal route using a novel 'poke and patch' approach to treat patients with trigger finger. This study may potentially revolutionize the treatment by making individualized splints with the capability to deliver drugs to treat trigger finger and other related health issues.

Acknowledgments

The authors thank the members of Kang Lab, National University of Singapore, Department of Pharmacy for their support and ideas throughout the project. There is no conflict of interests for any of the authors. This study was supported by the Singapore Ministry of Education (MOE) Academic Research Funding (AcRF) Tier 1 grant number R-148-000-207-112.

References

[1] Moore J S 2000 Flexor tendon entrapment of the digits (trigger finger and trigger thumb) *J. Occup. Environ. Med.* **42** 526
[2] Rayan G M 1990 Distal stenosing tenosynovitis *J. Hand Surg. Am.* **15** 973
[3] Rhoades C E, Gelberman R H and Manjarris J F 1984 Stenosing tenosynovitis of the fingers and thumb. Results of a prospective trial of steroid injection and splinting *Clin. Orthop. Relat. Res.* **190** 236–38
[4] Weilby A 1970 Trigger finger. Incidence in children and adults and the possibility of a predisposition in certain age groups *Acta Orthop. Scand.* **41** 419
[5] Ryzewicz M and Wolf J M 2006 Trigger digits: principles, management, and complications *J. Hand Surg. Am.* **31** 135
[6] Sampson S P, Badalamente M A, Hurst L C and Seidman J 1991 Pathobiology of the human A1 pulley in trigger finger *J. Hand Surg. Am.* **16** 714
[7] Sbernardori M C and Bandiera P 2007 Histopathology of the A1 pulley in adult trigger fingers *J. Hand Surg. Eur.* **32** 556
[8] Ametewee K 1983 Trigger thumb in adults after hyperextension injury *Hand* **15** 103
[9] Bonnici A V and Spencer J D 1988 A survey of 'trigger finger' in adults *J. Hand Surg. Br.* **13** 202
[10] Verdon M E 1996 Overuse syndromes of the hand and wrist *Prim. Care* **23** 305
[11] Fahey J J and Bollinger J A 1954 Trigger-finger in adults and children *J. Bone Joint Surg. Am.* **36-A** 1200
[12] Akhtar S, Bradley M J, Quinton D N and Burke F D 2005 Management and referral for trigger finger/thumb *Br. Med. J.* **331** 30

[13] Makkouk A H, Oetgen M E, Swigart C R and Dodds S D 2008 Trigger finger: etiology, evaluation, and treatment *Curr. Rev. Musculoskeletal Med.* **1** 92
[14] Group T W B, Mobile cellular subscriptions (per 100 people) | Data (http://data.worldbank.org/indicator/IT.CEL.SETS.P2)
[15] Patel M R and Bassini L 1992 Trigger fingers and thumb: when to splint, inject, or operate *J. Hand Surg. Am.* **17** 110
[16] Colbourn J, Heath N, Manary S and Pacifico D 2008 Effectiveness of splinting for the treatment of trigger finger *J. Hand Ther.* **21** 336
[17] Swezey R L 1999 Trigger finger splinting *Orthopedics* **22** 180
[18] Rodgers J A, McCarthy J A and Tiedeman J J 1998 Functional distal interphalangeal joint splinting for trigger finger in laborers: a review and cadaver investigation *Orthopedics* **21** 305
[19] Kameyama M, Meguro S, Funae O, Atsumi Y and Ikegami H 2009 The presence of limited joint mobility is significantly associated with multiple digit involvement by stenosing flexor tenosynovitis in diabetics *J. Rheumatol.* **36** 1686
[20] Shorr R I, Ray W A, Daugherty J R and Griffin M R 1993 Concurrent use of nonsteroidal anti-inflammatory drugs and oral anticoagulants places elderly persons at high risk for hemorrhagic peptic ulcer disease *Arch. Intern. Med.* **153** 1665
[21] Chan T 1995 Adverse interactions between warfarin and nonsteroidal antiinflammatory drugs: mechanisms, clinical significance, and avoidance *Ann. Pharmacother.* **29** 1274
[22] Houston M C 1991 Nonsteroidal anti-inflammatory drugs and antihypertensives *Am. J. Med.* **90** 42
[23] Pavlicevic I, Kuzmanic M, Rumboldt M and Rumboldt Z 2008 Interaction between antihypertensives and NSAIDs in primary care: a controlled trial *The Canadian journal of clinical pharmacology* **15** e372
[24] de Jong J C, van den Berg P B, Tobi H and de Jong-van den Berg L T 2003 Combined use of SSRIs and NSAIDs increases the risk of gastrointestinal adverse effects *Br. J. Clin. Pharmacol.* **55** 591
[25] Warner-Schmidt J L, Vanover K E, Chen E Y, Marshall J J and Greengard P 2011 Antidepressant effects of selective serotonin reuptake inhibitors (SSRIs) are attenuated by antiinflammatory drugs in mice and humans *Proc. Natl Acad. Sci. USA* **108** 9262
[26] Hippisley-Cox J and Coupland C 2005 Risk of myocardial infarction in patients taking cyclo-oxygenase-2 inhibitors or conventional non-steroidal anti-inflammatory drugs: population based nested case-control analysis *Br. Med. J.* **330** 1366
[27] Loke Y K, Trivedi A N and Singh S 2008 Meta-analysis: gastrointestinal bleeding due to interaction between selective serotonin uptake inhibitors and non-steroidal anti-inflammatory drugs *Aliment. Pharmacol. Ther.* **27** 31
[28] Helin-Salmivaara A, Huttunen T, Gronroos J M, Klaukka T and Huupponen R 2007 Risk of serious upper gastrointestinal events with concurrent use of NSAIDs and SSRIs: a case–control study in the general population *Eur. J. Clin. Pharmacol.* **63** 403
[29] Colebatch A N, Marks J L and Edwards C J 2011 Safety of non-steroidal anti-inflammatory drugs, including aspirin and paracetamol (acetaminophen) in people receiving methotrexate for inflammatory arthritis (rheumatoid arthritis, ankylosing spondylitis, psoriatic arthritis, other spondyloarthritis) *Cochrane Database Syst. Rev.* **11** CD008872
[30] Antman E M, Bennett J S, Daugherty A, Furberg C, Roberts H and Taubert K A 2007 Use of nonsteroidal antiinflammatory drugs an update for clinicians: a scientific statement from the American Heart Association *Circulation* **115** 1634
[31] Pope J E, Anderson J J and Felson D T 1993 A meta-analysis of the effects of nonsteroidal anti-inflammatory drugs on blood pressure *Arch. Intern. Med.* **153** 477
[32] Trelle S, Reichenbach S, Wandel S, Hildebrand P, Tschannen B, Villiger P M, Egger M and Juni P 2011 Cardiovascular safety of non-steroidal anti-inflammatory drugs: network meta-analysis *Br. Med. J.* **342** c7086
[33] Haag M D, Bos M J, Hofman A, Koudstaal P J, Breteler M M and Stricker B H 2008 Cyclooxygenase selectivity of nonsteroidal anti-inflammatory drugs and risk of stroke *Arch. Intern. Med.* **168** 1219
[34] Cryer B 1999 Nonsteroidal anti-inflammatory drug gastrointestinal toxicity *Curr. Opin. Gastroenterol.* **15** 473
[35] Patrono C and Dunn M J 1987 The clinical significance of inhibition of renal prostaglandin synthesis *Kidney Int.* **32** 1
[36] Perazella M A 2002 COX-2 selective inhibitors: analysis of the renal effects *Expert Opin. Drug Saf.* **1** 53
[37] Schneider V, Levesque L E, Zhang B, Hutchinson T and Brophy J M 2006 Association of selective and conventional nonsteroidal antiinflammatory drugs with acute renal failure: a population-based, nested case–control analysis *Am. J. Epidemiol.* **164** 881
[38] Rodríguez L A G, Williams R, Derby L E, Dean A D and Jick H 1994 Acute liver injury associated with nonsteroidal anti-inflammatory drugs and the role of risk factors *Arch. Intern. Med.* **154** 311
[39] Tarazi E M, Harter J G, Zimmerman H J, Ishak K G and Eaton R A 1993 Sulindac-associated hepatic injury: analysis of 91 cases reported to the Food and Drug Administration *Gastroenterology* **104** 569
[40] Rabinovitz M and Van Thiel D H 1992 Hepatotoxicity of nonsteroidal anti-inflammatory drugs *Am. J. Gastroenterol.* **87** 1696
[41] Aithal G P and Day C P 2007 Nonsteroidal anti-inflammatory drug-induced hepatotoxicity *Clin. Liver Dis.* **11** 563
[42] Rubenstein J H and Laine L 2004 Systematic review: the hepatotoxicity of non-steroidal anti-inflammatory drugs *Aliment Pharmacol. Ther.* **20** 373
[43] Shakeel M, Pathan Dilnawaz N, Ziyaurrrahman A, Akber B and Bushra S 2011 Microneedle as a novel drug delivery system: a review *Int. Res. J. Pharm.* **2** 72
[44] Kathuria H, Kochhar J S, Fong M H M, Hashimoto M, Iliescu C, Yu H and Kang L 2015 Polymeric microneedle array fabrication by photolithography *J. Vis. Exper.* **105** e52914
[45] Lahiji S F, Dangol M and Jung H 2015 A patchless dissolving microneedle delivery system enabling rapid and efficient transdermal drug delivery *Sci. Rep.* **5** 7914
[46] Kaushik S, Hord A H, Denson D D, McAllister D V, Smitra S, Allen M G and Prausnitz M R 2001 Lack of pain associated with microfabricated microneedles *Anesthesia Analgesia* **92** 502
[47] Xie Y, Xu B and Gao Y 2005 Controlled transdermal delivery of model drug compounds by MEMS microneedle array *Nanomed.: Nanotechnol. Biol. Med.* **1** 184
[48] Cai B, Xia W, Bredenberg S, Li H and Engqvist H 2015 Bioceramic microneedles with flexible and self-swelling substrate *Eur. J. Pharm. Biopharm.* **94** 404
[49] Choi C K, Kim J B, Jang E H, Youn Y N and Ryu W H 2012 Curved biodegradable microneedles for vascular drug delivery *Small* **8** 2483
[50] Kim M, Kim T, Kim D S and Chung W K 2015 Curved microneedle array-based sEMG electrode for robust long-term measurements and high selectivity *Sensors* **15** 16265
[51] Matsuda T and Mizutani M 2002 Liquid acrylate-endcapped biodegradable poly (ϵ-caprolactone-co-trimethylene carbonate). II. Computer-aided stereolithographic microarchitectural surface photoconstructs *J. Biomed. Mater. Res.* **62** 395
[52] Giannatsis J and Dedoussis V 2009 Additive fabrication technologies applied to medicine and health care: a review *Int. J. Adv. Manuf. Technol.* **40** 116
[53] Kim Y-C, Park J-H and Prausnitz M R 2012 Microneedles for drug and vaccine delivery *Adv. Drug. Deliv. Rev.* **64** 1547
[54] Shivanand P, Binal P and Viral D 2009 Microneedles: progress in developing new technology for painless drug delivery *Int. J. Pharmtech Res.* **1** 1279
[55] Kochhar J S, Quek T C, Soon W J, Choi J, Zou S and Kang L 2013 Effect of microneedle geometry and supporting substrate on microneedle array penetration into skin *J. Pharm. Sci.* **102** 4100

[56] Martini F and Nath J L 2008 *Fundamentals of Anatomy and Physiology* (San Fransisco: Pearson)
[57] Khanna P, Luongo K, Strom J A and Bhansali S 2010 Axial and shear fracture strength evaluation of silicon microneedles *Microsyst. Technol.* **16** 973
[58] Larrañeta E, Moore J, Vicente-Pérez E M, González-Vázquez P, Lutton R, Woolfson A D and Donnelly R F 2014 A proposed model membrane and test method for microneedle insertion studies *Int. J. Pharm.* **472** 65
[59] Hamzah A A, Aziz N A, Majlis B Y, Yunas J, Dee C F and Bais B 2012 Optimization of HNA etching parameters to produce high aspect ratio solid silicon microneedles *J. Micromech. Microeng.* **22** 095017
[60] Lu Y, Mantha S N, Crowder D C, Chinchilla S, Shah K N, Yun Y H, Wicker R B and Choi J W 2015 Microstereolithography and characterization of poly(propylene fumarate)-based drug-loaded microneedle arrays *Biofabrication* **7** 045001
[61] Predel H G, Giannetti B, Pabst H, Schaefer A, Hug A M and Burnett I 2013 Efficacy and safety of diclofenac diethylamine 1.16% gel in acute neck pain: a randomized, double-blind, placebo-controlled study *BMC Musculoskeletal Disord.* **14** 250
[62] Zhang Y, Brown K, Siebenaler K, Determan A, Dohmeier D and Hansen K 2012 Development of lidocaine-coated microneedle product for rapid, safe, and prolonged local analgesic action *Pharm. Res.* **29** 170
[63] Kochhar J S, Anbalagan P, Shelar S B, Neo J K, Iliescu C and Kang L 2014 Direct microneedle array fabrication off a photomask to deliver collagen through skin *Pharm. Res.* **31** 1724
[64] Markovic M, Van Hoorick J, Holzl K, Tromayer M, Gruber P, Nurnberger S, Dubruel P, Van Vlierberghe S, Liska R and Ovsianikov A 2015 Hybrid tissue engineering scaffolds by combination of three-dimensional printing and cell photoencapsulation *J. Nanotechnol. Eng. Med.* **6** 0210011
[65] Skoog S A, Goering P L and Narayan R J 2014 Stereolithography in tissue engineering *J. Mater. Sci., Mater. Med.* **25** 845
[66] Chia H N and Wu B M 2015 Recent advances in 3D printing of biomaterials *J. Biol. Eng.* **9** 4
[67] Kim G B *et al* 2016 Three-dimensional printing: basic principles and applications in medicine and radiology *Korean J. Radiol.* **17** 182